Calculation of Cogging Force in Permanent Magnet Linear Motor Using Analytical and Finite Element Methods

Mohammad Reza Zare[1,2] Mousa Marzband[3]
1- Islamic Azad University Majlesi Branch, Isfahan, Iran
2- Department of Electrical & Electronic, Faculty of Engineering, University Putra Malaysia
Email: m.r.zare@ieee.org
3- Islamic Azad University lahijan Branch
Email: m_marzband2005@yahoo.com

Received: May 2010 Revised: July 2010 Accepted: September 2010

ABSTRACT:
In a permanent magnet (PM) linear motor, there is a force ripple which is detrimental to positioning. This force ripple is mainly due to a cogging force and a mutual force ripple. These forces are affected by the geometric parameters of a brushless PM motor, such as the width of the magnet, the height of the magnet, the shifted length of the magnetic pole, the length and height of the armature and the slot width. The optimal design can be found by considering force ripple as a cost function and the geometric parameters as design variables. In this paper, we calculate the flux density distribution in the air gap using the analytic solution of Laplace and Possion equations in the function of geometric parameters. The cogging force is obtained by integrating the Maxwell stress tensor, which is described by the flux density distribution on the slot face and end face of the iron core of an armature. Finally, a finite element method is presented in order to compare with the previous method.

KEYWORDS: Linear Brushless Permanent Magnet Motor, Cogging Force, Thrust force, Analytical methods, finite element method.

1. INTRODUCTION

In a brushless permanent magnet (PM) motor with salient-poles, there is a force ripple which is detrimental to positioning. This force ripple is mainly due to a cogging force and a mutual force ripple. In a rotary PM motor, the cogging force is generated by the interaction of the rotor magnetic field with the stator magnetic reluctance. On the other hand the mutual force ripple is generated by the interaction of an excitation current MMF (Magneto-Motive Force) with the magnetic field or rotor magnetic reluctance [1, 2]. In a linear PM motor, there are two components of the cogging force. One is a tooth ripple component, which also exists in a rotary motor. The other one is an end-effect component, which exists only in a linear motor and is caused by the finite length of the armature. The method for minimizing the force ripple has been studied by many researchers. The tooth ripple component of the cogging force can be reduced by skewing the magnet or armature [3]. Optimizing the shifted length of the magnet pole and the ratio of the magnet width to pole pitch also reduce the tooth ripple [4]. The end-effect component of the cogging force can be minimized by optimizing the armature length [5]. The mutual force ripple can be reduced by matching the current waveform with the magnetic field distribution [6]. These methods use data from a finite element analysis (FEA) to reduce force ripple [1, 4, 5]. The flux density distribution can be described by geometric parameters that are related to the force ripple. The force ripple is also described by the flux density distribution. Therefore the optimal design can be found by considering force ripple as a cost function and the geometric parameters as design variables. The cogging force is obtained by integrating the Maxwell stress tensor, which is described by the flux density distribution on the slot face and the end face of the iron core of armature.

2. GEOMETRICAL STRUCTURE AND ANALYTICAL MODEL

Figure 1 shows the basic geometrical structure of a linear brushless PM motor. The iron core of the armature is wound by a coil with three phases. The stator is attached to permanent magnets and it is faced with an armature winding with N and S poles. The parameters of the linear brushless PM motor are listed in Table 1. Among these parameters, the geometric parameters, used as design variables, are

width of magnet (ω_M), height of magnet (h_M), length of armature (l_A), height of armature (h_A) and slot width (ω_S). In order to simplify the field analysis, a two-dimensional model is adapted to include an air gap and a magnet. The permeability of the iron core and the stator is assumed to be infinite. Therefore the flux density has only the normal component at the surface of the iron core and stator. Figure 2 shows the simplified model for the analysis of the magnet and air gap fields [7].

Table 1. Geometric parameters of the motor

Parameter	Symbol	Value (unit)
Slot pitch	τ_s	**8 [mm]**
Slot width	ω_s	**4 [mm]**
Armature height	h_A	**14-22 [mm]**
Armature length	l_A	**140-148 [mm]**
Pole pitch	τ	**24 [mm]**
Magnet height	h_M	**10 [mm]**
Magnet width	ω_M	**14.4-24 [mm]**
Air gap length	δ	**1 [mm]**

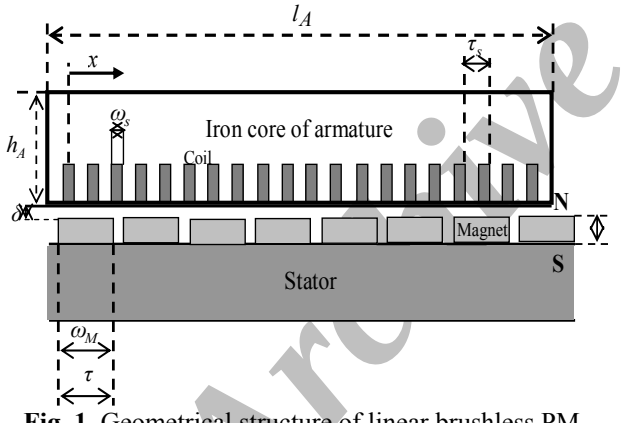

Fig. 1. Geometrical structure of linear brushless PM motor

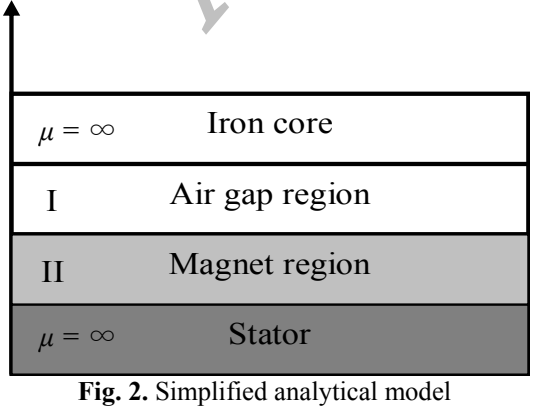

Fig. 2. Simplified analytical model

3. ANALYTICAL REPRESENTATION OF COGGING FORCE

In order to obtain the cogging force, an analytical method is presented as follows. The simplified analytical model of Figure 2 can be expressed in terms of magnetic vector potential. In the air gap region, the Laplace equation is

$$\frac{\partial^2 A_I}{\partial x^2} + \frac{\partial^2 A_I}{\partial y^2} = 0 \tag{1}$$

In the magnet region, the Possion equation is

$$\frac{\partial^2 A_{II}}{\partial x^2} + \frac{\partial^2 A_{II}}{\partial y^2} = \mu_M J_M \tag{2}$$

Where A_I and A_{II} are the magnetic vector potential of the each region, μ_M is the permeability of the magnet and J_M is the distribution of current density in the current sheet model, which generates a magnetic field equivalent to the magnets [8]. The current density can be expressed as a function of magnet geometry and properties as follows.

$$J_M(x) = \frac{B_r}{\mu_M} \sum_{n=1,3,5,..}^{\infty} \frac{4}{\tau} \sin(\frac{\alpha n \pi}{2}) \sin(\frac{n \pi x}{\tau}) \tag{3}$$

Where B_r is the permanent magnetic flux density, τ is the pole pitch and α is the ratio of width of the magnet to the pole pitch.

The corresponding general solutions of equations (1), (2) are given by [9]

$$A_I(x) = \sum (C_1 \times e^{\frac{n\pi y}{\tau}} + C_2 \times e^{\frac{n\pi y}{\tau}}) \times \sin(\frac{n\pi x}{\tau}) \tag{4}$$

$$A_{II}(x) = \sum (C_3 \times e^{\frac{n\pi y}{\tau}} + C_4 \times e^{\frac{n\pi y}{\tau}} + \frac{4B_r \tau}{n^2 \pi^2} \times \sin(\frac{\alpha n \pi}{2})) \times \sin(\frac{n\pi x}{\tau}) \tag{5}$$

From the assumption that the permeability of the iron core and stator is infinite, the boundary conditions must be satisfied by equations (4) and (5).

$$Aty = \delta : \qquad H_{xI} = 0$$

$$Aty = 0 : \quad H_{xII} = H_{xI} \quad and \quad B_{yII} = B_{yI}$$

$$Aty = h_M : \qquad H_{xII} = 0$$

From these boundary conditions, the constants of equations (4) and (5) can be determined by:

$$C_1 = C_2 \times e^{-\frac{2n\pi\delta}{\tau}}$$

$$C_2 = \frac{\frac{4B_r\tau}{n^2\pi^2}\times\sin(\frac{\alpha n\pi}{2})}{(e^{\frac{2n\pi\delta}{\tau}}+1)+\frac{\mu_M(e^{\frac{2n\pi\delta}{\tau}}+1)(e^{\frac{2n\pi h_M}{\tau}}+1)}{\mu_0(e^{\frac{2n\pi h_M}{\tau}}-1)}}$$

$$C_3 = C_4 e^{-\frac{2n\pi h_M}{\tau}}$$

$$C_4 = \frac{\mu_M(e^{\frac{2n\pi\delta}{\tau}}+1)}{\mu_0(e^{\frac{2n\pi h_M}{\tau}}-1)}$$

Where h_M is the height of the magnet and δ is the air gap length.

Flux density distribution can be derived by curling the magnetic vector potential. As the direction of the magnetic vector potential is normal to the XY plane, the flux density distribution is

$$\vec{B} = \nabla \times \vec{A}$$

$$=(\frac{\partial}{\partial x}\vec{i}+\frac{\partial}{\partial x}\vec{j}+\frac{\partial}{\partial x}\vec{k})\times A\vec{k} \quad (6)$$

$$=\frac{\partial A}{\partial x}\vec{i}+\frac{\partial A}{\partial x}\vec{j}$$

In equation (6), the flux density distribution on the iron core of the armature is interfaced with the air gap and since it has only a normal component, it is given by

$$B_y(x) = \frac{\partial A_I}{\partial x} = \sum_{n=1,3,5,\ldots}^{\infty}\frac{n\pi}{\tau}(C_1 e^{\frac{n\pi\delta}{\tau}}+C_2 e^{-\frac{n\pi\delta}{\tau}})\cos(\frac{n\pi x}{\tau}) \quad (7)$$

The slot on the iron core of the armature changes the length of the gap with the equivalent radius [10]. So the flux density distribution is modified by the slot which is given by

$$B_{ys}(x) = \alpha_s \sum\frac{n\pi}{\tau}(C_1 e^{\frac{n\pi y}{\tau}}+C_2 e^{-\frac{n\pi y}{\tau}})\cos(\frac{n\pi x}{\tau})$$

$$\alpha_s = \frac{\mu_M\delta+h_M}{\mu_M\delta+h_M+0.5\mu_M\pi r_s} \quad (8)$$

$$for \quad (k-1)\tau_s - \frac{w_s}{2} \le x \le (k-1)\tau_s + \frac{w_s}{2}$$

$$k = 1,2,3,\ldots,Q_s$$

Where τ_S is the slot pitch, ω_S is the slot width, r_S is the function of x and Q_S is the number of slots.

The cogging force is obtained by integrating the Maxwell stress tensor along the slot face on the iron core of the armature [11]. By assumption, the flux density distribution has only the normal component at the surface of the iron core as in Figure 3. From the flux density distribution, the normal and tangential forces acting on each surface of the armature are given by

$$F_n = \frac{L}{2\mu_0}\int[B_n^2 - B_t^2]dl = \frac{L}{2\mu_0}\int B_n^2 dl \quad (9)$$

$$F_n = \frac{L}{\mu_0}\int B_n B_t dl = 0 \quad (10)$$

Where L is the effective length of the armature coil and l is an integral path along the surface.

The tooth ripple component of the cogging force is calculated by summation of the normal forces at each slot area. In equation (11), F_{1K} is the rightward force component and F_{2K} is the leftward force component in k-th slot. The waveform of this cogging force has a period of the slot pitch and can be reduced by changing the ratio of magnet width to the pole pitch as in Figure 4.

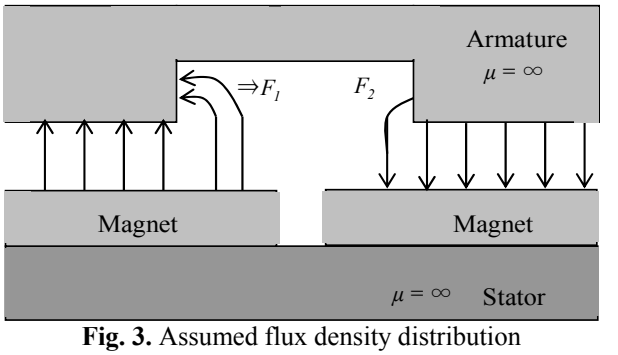

Fig. 3. Assumed flux density distribution

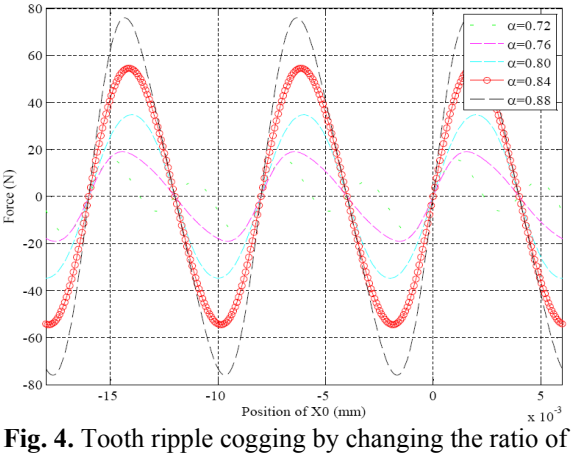

Fig. 4. Tooth ripple cogging by changing the ratio of the magnet width to the pole pitch

$$F_n(x_0) = \sum_{k=1}^{Q_S} F_k(x_0) = \Sigma(F_{1k}(x_0) \quad F_{2k}(x_0))$$

$$= \frac{L}{4\mu_0} \sum_{k=1}^{Q_S} \{[\sum_{n=1,3,...}^{\infty} B_{sn}^2 (x_{12} \quad x_{11} + \frac{\tau}{2n\pi} (\sin(\frac{2n\pi x_{12}}{\tau})$$

$$\sin(\frac{2n\pi x_{11}}{\tau}))$$

$$+ \sum_{\substack{n=1,3,.. \\ m=n+2,..}} B_{sn} B_{sm} (\frac{\tau}{(n \quad m)\pi} (\sin(\frac{(n \quad m)\pi x_{12}}{\tau})$$

$$\sin(\frac{(n \quad m)\pi x_{11}}{\tau})))$$

$$+ (\frac{\tau}{(n+m)\pi} (\sin(\frac{(n+m)\pi x_{12}}{\tau}) \quad \sin(\frac{(n+m)\pi x_{11}}{\tau})))$$

$$[\sum_{n=1,3,5,...}^{\infty} B_{sn}^2 (x_{22} \quad x_{21} + \frac{\tau}{2n\pi} (\sin(\frac{2n\pi x_{22}}{\tau}) \quad \sin(\frac{2n\pi x_{21}}{\tau})))$$

$$+ \sum_{\substack{n=1,3,.. \\ m=n+2,..}} B_{sn} B_{sm} (\frac{\tau}{(n \quad m)\pi} (\sin(\frac{(n \quad m)\pi x_{22}}{\tau}) \quad \sin(\frac{(n \quad m)\pi x_{21}}{\tau})))$$

$$+ (\frac{\tau}{(n+m)\pi} (\sin(\frac{(n+m)\pi x_{22}}{\tau}) \quad \sin(\frac{(n+m)\pi x_{21}}{\tau})))$$

$$B_{sn} = \frac{n\pi}{\tau} (C_1 e^{\frac{n\pi\delta}{\tau}} + C_2 e^{\frac{n\pi\delta}{\tau}})$$

$$B_{sm} = \frac{n\pi}{\tau} (C_1 e^{\frac{m\pi\delta}{\tau}} + C_2 e^{\frac{m\pi\delta}{\tau}})$$

$$x_{11} = x_0 + (k \quad 1)\tau_s \quad \frac{w_s}{2}, \qquad (11)$$

$$x_{12} = x_0 + (k \quad 1)\tau_s$$

$$x_{21} = x_0 + (k \quad 1)\tau_s,$$

$$x_{22} = x_0 + (k \quad 1)\tau_s \quad \frac{w_s}{2}$$

where x_0 is an armature position relative to the magnet poles.

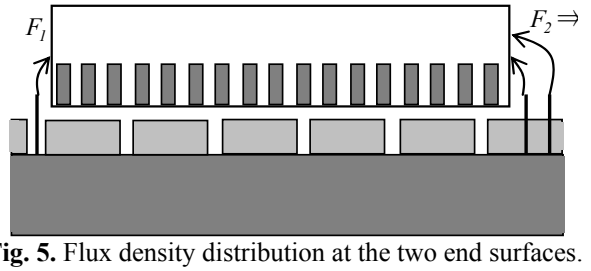

Fig. 5. Flux density distribution at the two end surfaces.

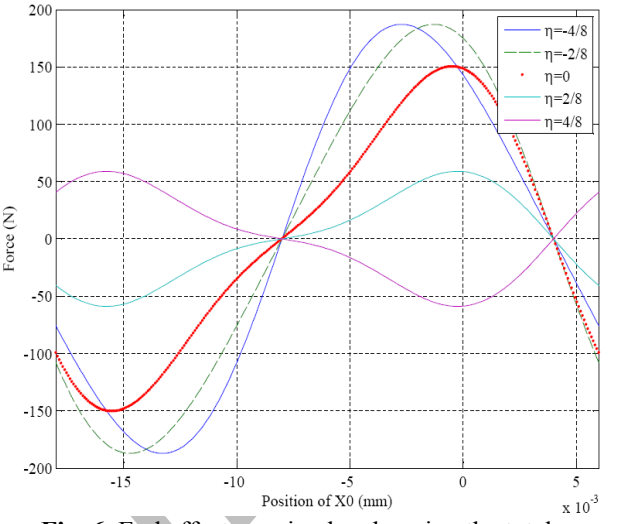

Fig. 6. End effect cogging by changing the total armature length of the iron core.

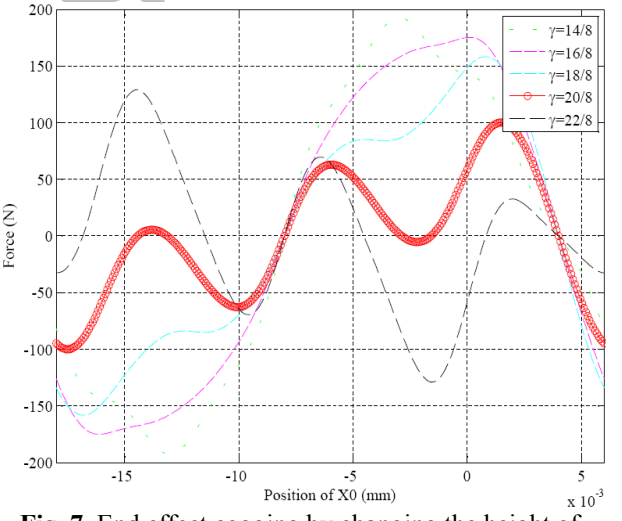

Fig. 7. End effect cogging by changing the height of the iron core.

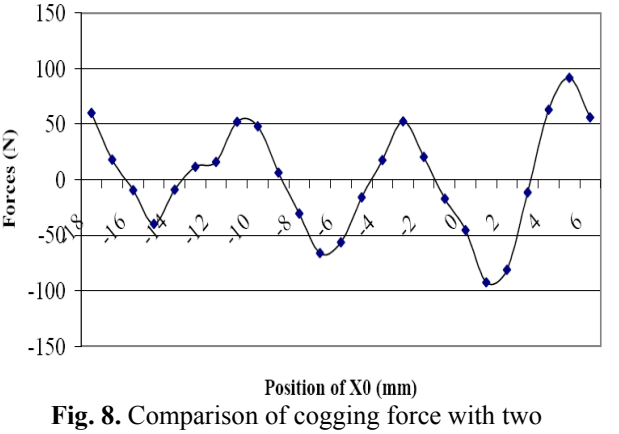

Fig. 8. Comparison of cogging force with two components of tooth ripples and end effect.

$$F_n(x) = F_k(x) = (F_{1k}(x) \quad F_{2k}(x)$$

$$= \frac{L}{4\mu_0}\{[\sum_{n=1,3,5,\ldots}^{\infty} B_{sn}^2 (x_{12} \quad x_{11} + \frac{\tau}{2n\pi}(\sin(\frac{2n\pi x_{12}}{\tau})$$

$$\sin(\frac{2n\pi x_{11}}{\tau})))$$

$$+ \sum_{\substack{n=1,3,..\\ m=n+2,..}} B_{sn} B_{sm} (\frac{\tau}{(n \quad m)\pi}(\sin(\frac{(n \quad m)\pi x_{12}}{\tau})$$

$$\sin(\frac{(n \quad m)\pi x_{11}}{\tau}))) + (\frac{\tau}{(n+m)\pi}(\sin(\frac{(n+m)\pi x_{12}}{\tau})$$

$$\sin(\frac{(n+m)\pi x_{11}}{\tau})))$$

$$[\sum_{n=1,3,5,\ldots}^{\infty} B_{sn}^2 (x_{22} \quad x_{21} + \frac{\tau}{2n\pi}(\sin(\frac{2n\pi x_{22}}{\tau})$$

$$\sin(\frac{2n\pi x_{21}}{\tau})))$$

$$+ \sum_{\substack{n=1,3,..\\ m=n+2,..}} B_{sn} B_{sm} (\frac{\tau}{(n \quad m)\pi}(\sin(\frac{(n \quad m)\pi x_{22}}{\tau})$$

$$\sin(\frac{(n \quad m)\pi x_{21}}{\tau}))) + (\frac{\tau}{(n+m)\pi}(\sin(\frac{(n+m)\pi x_{22}}{\tau})$$

$$\sin(\frac{(n+m)\pi x_{21}}{\tau})))$$

$$x_{11} = x_0 - \frac{w_s}{2} \quad \frac{\tau_s}{2} \quad d_t \quad h_A$$

$$x_{12} = x_0 - \frac{w_s}{2} \quad \frac{\tau_s}{2} \quad d_t \qquad (12)$$

$$x_{21} = x_0 + (Q_s \quad 1)\tau_s + \frac{w_s}{2} + \frac{\tau_s}{2} + d_t$$

$$x_{22} = x_0 + (Q_s \quad 1)\tau_s + \frac{w_s}{2} + \frac{\tau_s}{2} + d_t + h_A$$

The end effect component of the cogging force is calculated by summation of the normal force at the two ends of iron core in the equation (12). The flux density distribution at the two end surfaces is shown in Figure 5. This force is related to height and total length of the iron core and it has the period of the pole pitch. So a reduction of this force can be achieved by changing the total length of the iron core and the height of the iron core according to $l_A = (n+\eta)\tau S$ and $h_A = \gamma\tau S$,where n is an integer, η is the ratio of increase of length to slot pitch and γ is the ratio of height of the iron core to the slot pitch as seen in Figures 6 and 7. In addition, this force can be changed by shifting the magnet pole and by changing the ratio of magnet width to pole pitch. Where h_A is the height of iron core and d_t is the increase in the total length of iron core. Figure 8 shows a comparison of the end-effect cogging and the cogging force with two components at the one pole pitch.

4. FINITE ELEMENT METHOD

Here a PM linear motor three dimensional model is presented. The model was designed by using the existing characteristics in Table 1. The designed model is shown in Figure 9.

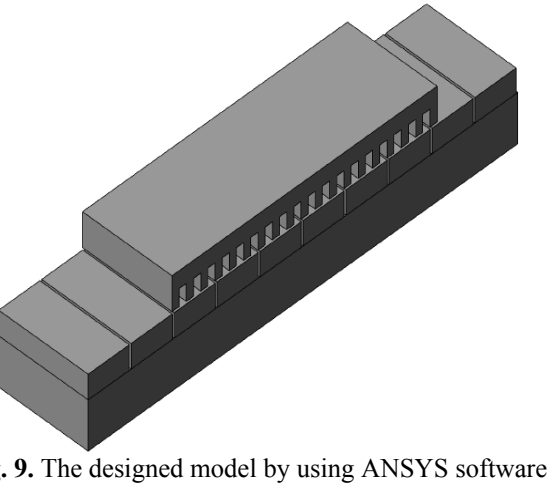

Fig. 9. The designed model by using ANSYS software

In Figure 10, the flux density before current injection in the system is shown. The flux density is high at certain points including the distance between the slot head and the magnet which is located over the stator.

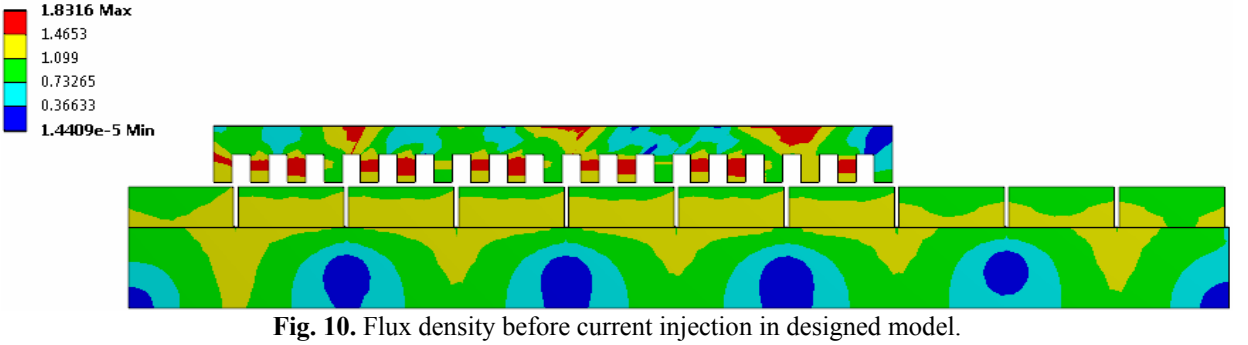

Fig. 10. Flux density before current injection in designed model.

Figure 11 shows the cogging force obtained with attention to the changing of movement X_0 between -18 to 6 at a one pole pitch.

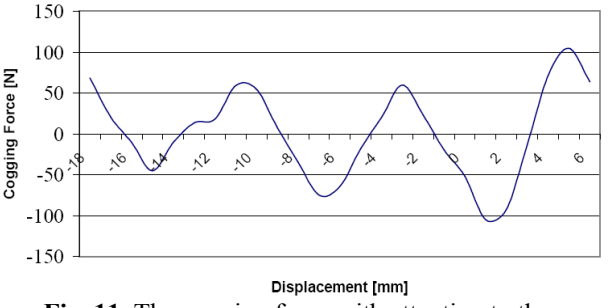

Fig. 11. The cogging force with attention to the changing of movement

Figure 12 shows the comparison between two aforesaid methods. The deviation of the presented methods is almost 12%.

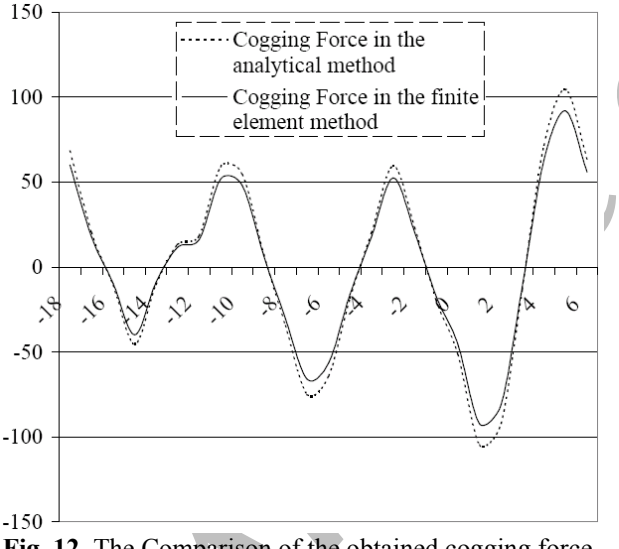

Fig. 12. The Comparison of the obtained cogging force by the two mentioned methods

5. CONCLUSIONS

The flux density distribution in the air gap is represented by an analytic solution of Laplace's equation and Possion equation. This flux density distribution is described as a function of the motor geometric parameters, such as the width of the magnet, the height of the magnet, the length of the armature, the height of the armature and the slot width. The cogging force is obtained by integrating the Maxwell stress tensor, which is calculated from the flux density distribution on the slot face and the end face of the iron core of the armature.

From the developed analytical model, the optimal design for reducing the cogging force in a linear brushless PM motor can be determined. In the optimal design, the geometric parameters of motor can be considered as design variables.

It is found that the cogging force determined by analytical method agrees fairly well with those obtained by finite element analysis, although minor deviation (12%) exists.

REFERENCES

[1] Z. Q. Zhu et al., "**Calculation of cogging force in a novel slotted linear tubular brushless permanent magnet motor**", *IEEE Trans. on Magnetics*, Vol. 33, No. 5, pp 4098-4100, (September 1997)

[2] Tomas M. Jahns et al., "**Pulsating torque minimization techniques for permanent magnet AC motor drives-a review**", *IEEE Trans. Ind. Electronics*, Vol. 43, No. 2, pp. 321-330 (April 1996)

[3] Jaime De La Ree and Nady Boules, "**Torque production in permanent-magnet synchronous motors**", *IEEE Trans. Ind. Applications*, Vol. 25, No. 1, pp. 107-112, (January/February 1989)

[4] Touzhu Li and Gordon Slemon, "**Reduction of cogging torque in permanent magnet motors**", *IEEE Trans. on Magnetics*, Vol. 24, No. 6, pp. 2901-2903, (November 1988)

[5] Z. Q. Zhu et al., "**Reduction of cogging force in slotless linear permanent magnet motors**", *IEE Proc-Electr. Power Appl.*., Vol.144, No. 4, pp.277-282 , (July 1997)

[6] J. Hung and Z. Ding, "**Design of current to reduce torque ripple in brushless permanent magnet motors**", *IEE Proc.*, Vol. 140, No. 4, pp.260-266, (July 1993)

[7] Myung J. Chung, Moon G. Lee, Sung Q Lee, Sun M. Kim, and Dae-Gab Gweon, "**Analytical Representation of Cogging Force in Linear Brushless Permanent Magnet Motor**", *Technical Report, Korea Advanced Institute of Science and Technology*

[8] N. Boules, "**Impact of slot harmonics on losses of high-speed permanent machines with a magnet retaining ring**", *Elec. Mach. and Electromech.*, Vol. 6, pp.527-539, (Nov. 1981)

[9] K. J. Binns and P. J. Lawrenson, "**Analysis and computation of electric and magnetic field problems**", *Pergamon press*, p.95, (1973)

[10] Z. Q. Zhu and D. Howe, "**Analytical prediction of the cogging torque in radial-field permanent magnet brushless motors**", *IEEE Trans. on Magnetics*, Vol. 28, No. 2, pp. 1371-1374, (March 1992)

[11] Jacek F. Gieras and Mitchell Wing, "**Permanent magnet motor technology - Design and Applications**", *Marcel Dekker Inc.*, p.88, (1997)

[12] J. G. Gieras and Z. J. Piech, "**Linear Synchronous Motors. Boca Raton**", *FL: CRC*, (2000)